A climatology of summer-time Arctic cyclones using a modified phase space

Croad, H. L., Methven, J. ORCID: https://orcid.org/0000-0002-7636-6872, Harvey, B. ORCID: https://orcid.org/0000-0002-6510-8181, Keeley, S. P. E., Volonté, A. ORCID: https://orcid.org/0000-0003-0278-952X and Hodges, K. I. ORCID: https://orcid.org/0000-0003-0894-229X (2023) A climatology of summer-time Arctic cyclones using a modified phase space. Geophysical Research Letters, 50 (22). e2023GL105993. ISSN 1944-8007 doi: https://doi.org/10.1029/2023GL105993 Available at https://centaur.reading.ac.uk/114160/

Geophysical Research Letters

RESEARCH LETTER
10.1029/2023GL105993

A Climatology of Summer-Time Arctic Cyclones Using a Modified Phase Space

Hannah L. Croad[1], John Methven[1], Ben Harvey[1,2], Sarah P. E. Keeley[3], Ambrogio Volonté[1,2], and Kevin I. Hodges[1,2]

[1]Department of Meteorology, University of Reading, Reading, UK, [2]National Centre for Atmospheric Science, University of Reading, Reading, UK, [3]European Centre for Medium-Range Weather Forecasts (ECMWF), Reading, UK

Key Points:

- Arctic cyclones in summer are classified by their vorticity structure during growth: low-level-dominant (LLD) or upper-level-dominant (ULD)
- LLD cyclones (65.5%) exhibit more warm-core baroclinic structures, preferentially track on the Russian coastline, and are typically stronger
- ULD cyclones (34.5%) exhibit more cold-core axisymmetric structures, preferentially track in the Pacific sector, and tend to be longer-lived

Correspondence to:
H. L. Croad,
h.croad@pgr.reading.ac.uk

Citation:
Croad, H. L., Methven, J., Harvey, B., Keeley, S. P. E., Volonté, A., & Hodges, K. I. (2023). A climatology of summer-time Arctic cyclones using a modified phase space. *Geophysical Research Letters*, *50*, e2023GL105993. https://doi.org/10.1029/2023GL105993

Received 25 AUG 2023
Accepted 6 NOV 2023

Author Contributions:
Conceptualization: Hannah L. Croad, John Methven, Ben Harvey, Ambrogio Volonté
Data curation: Ambrogio Volonté
Formal analysis: Hannah L. Croad
Investigation: Hannah L. Croad
Methodology: Hannah L. Croad
Project Administration: John Methven
Software: Kevin I. Hodges
Supervision: John Methven, Ben Harvey, Sarah P. E. Keeley, Ambrogio Volonté
Visualization: Hannah L. Croad
Writing – original draft: Hannah L. Croad
Writing – review & editing: John Methven, Ben Harvey, Sarah P. E. Keeley, Ambrogio Volonté, Kevin I. Hodges

Abstract We perform a climatological analysis of summer-time Arctic cyclone structure in reanalysis data using a phase space approach. A classification scheme for Arctic cyclones is proposed, dependent on whether vorticity structure during development is low-level-dominant (LLD) or upper-level-dominant (ULD). During growth, LLD cyclones (65.5%) exhibit warm-core asymmetric structures, whereas ULD cyclones (34.5%) have cold-core asymmetric structures. LLD cyclones typically have greater thermal asymmetry during growth. However, a transition to a persistent cold-core axisymmetric structure after maturity is characteristic of summer-time Arctic cyclones, regardless of structure during growth. LLD cyclones are typically stronger and preferentially track on the Russian coastline where there is high baroclinicity, whereas ULD cyclones tend to be longer-lived and preferentially track in the Pacific sector, where they can interact with tropopause polar vortices. This study provides a platform for further research into different classes of Arctic cyclones and associated hazardous weather, and ultimately for developing conceptual models.

Plain Language Summary We investigate the structure of cyclones, large-scale low-pressure systems, in the summer-time Arctic, using observations-based data of the atmosphere. A phase space is used to represent two aspects of cyclone structure, specifically (a) the low-level horizontal temperature contrast (i.e., whether there is a distinct warm sector), and (b) the vertical change in wind. We classify Arctic cyclones based on their vertical structure as they develop, as either low-level-dominant (LLD), where winds decrease with height, or upper-level-dominant (ULD), where winds increase with height. During growth, LLD cyclones (65.5%) exhibit warm-core structures whereas ULD cyclones (34.5%) have cold-core structures, both with strong low-level temperature contrasts. LLD cyclones tend to have a stronger warm sector contrast during development. However, after maximum intensity, when a cyclone matures and begins to weaken, both subsets of cyclones typically evolve to have long-lasting cold-core structures without a warm sector. LLD cyclones are typically stronger and preferentially track on the Russian coastline, whereas ULD cyclones tend to be longer-lived, and preferentially track in the Pacific sector of the Arctic. This study provides a platform for further research into different classes of Arctic cyclones, and ultimately for developing conceptual models, which are key for anticipating associated hazardous weather.

1. Introduction

Arctic cyclones are the major weather hazard to the increasing human activity in the summer-time Arctic (e.g., Babin et al., 2020; Li et al., 2021), and can be associated with extreme surface winds, ocean waves (e.g., Thomson & Rogers, 2014; Waseda et al., 2018, 2021), and the break-up and melting of sea ice (e.g., Asplin et al., 2012; Lukovich et al., 2021; Peng et al., 2021). Furthermore, Arctic cyclones in summer can be long-lived, exacerbating the impact of any associated hazards. For example, the great Arctic cyclone of 2012 (henceforth C12) lasted for almost 13 days (Simmonds & Rudeva, 2012), and an Arctic cyclone in August 2016 was maintained for over 1 month through repeated cyclone mergings (Yamagami et al., 2017).

The structural development of mid-latitude cyclones is well-established, with conceptual models such as the Norwegian (Bjerknes, 1919) and Shapiro-Keyser (Shapiro & Keyser, 1990) models, which are key for anticipating hazardous weather within a cyclone. However, the structural evolution of Arctic cyclones is not as well understood. Studies of extreme summer-time cases suggest that Arctic cyclones can have different structures to mid-latitude cyclones (e.g., Aizawa & Tanaka, 2016; Tanaka et al., 2012; Tao et al., 2017). However, climatological studies are needed to complement these works and assess how typical these cases are. Previously,

climatologies of Arctic cyclones (e.g., Vessey et al., 2020; Zhang et al., 2004) did not consider cyclone structure. In more recent work, Vessey et al. (2022) showed that summer-time Arctic cyclones undergo a transition at maximum intensity from a tilted baroclinic to an axisymmetric cold-core structure. However, the composite approach used did not permit for different varieties of cyclone structural evolution.

Gray et al. (2021) performed a climatological analysis of summer-time Arctic cyclones and tropopause polar vortices (TPVs), long-lived vortices on the tropopause which are common in the summer-time Arctic due to the lack of wind shear (Cavallo & Hakim, 2009, 2010). It was shown that Arctic cyclones that develop with a TPV ("matched") have a distinct structure to those that do not ("unmatched"). In a similar vein, Croad et al. (2023) focused on two summer-time cyclones with contrasting structure from summer 2020. Cyclone A (henceforth C20A) developed as a baroclinic wave along the northern coast of Russia on the Arctic frontal zone (AFZ; Day & Hodges, 2018; Serreze et al., 2001). The cyclone had a low-level-dominant (LLD) vorticity structure during development, with a structural evolution resembling a mid-latitude cyclone. In contrast, Cyclone B (henceforth C20B) developed with a TPV, with an upper-level-dominant (ULD) vorticity structure. Whilst Cyclone A had stronger winds, Cyclone B attained a cold-core columnar vortex structure that persisted for several days, looking quite different to a typical mid-latitude cyclone. The hypothesis is that cyclones A and B from Croad et al. (2023) represent two archetypal structural evolutions of Arctic cyclones.

Here we investigate summer-time Arctic cyclone structure using a modified form of the Hart (2003) cyclone phase space. This is a flexible approach to classifying cyclone structure, as it allows for a continuum of structures. In this study cyclones are categorized as having LLD or ULD development, determined by their vorticity structure at maximum growth rate. Note that this may have some similarities with the unmatched/matched classification from Gray et al. (2021), but here the focus is on general evolution of cyclone structure, rather than feature-based identification of TPVs. In this work we aim to answer the following:

1. What are the characteristic cyclone structures in the summer-time Arctic?
2. How does LLD/ULD growth determine subsequent cyclone structural evolution, and how frequently does each type of growth occur?
3. How is LLD/ULD growth related to cyclone strength, longevity, and location?

2. Methodology

2.1. Reanalysis Data

The study uses ERA5, the fifth-generation European Centre for Medium-Range Weather Forecasts (ECMWF) reanalysis data set (Hersbach et al., 2017, 2020), produced using the ECMWF's Integrated Forecasting System model cycle 41r2. The model has spectral truncation TL639 (~31 km horizontal grid spacing at the equator), and 137 terrain-following hybrid-pressure levels from the surface to 0.01 hPa. 6-hourly data on a 0.25° regular latitude-longitude grid during 1979–2021 is used.

2.2. Arctic Cyclone Tracking

Arctic cyclone tracks are identified from ERA5 data using the TRACK algorithm (Hodges, 1994, 1995, 2021). This is employed on 1-hourly spectrally truncated (T5-63; removing total wavenumbers less than 5 and more than 63) 850 hPa relative vorticity (ξ_{850}). Maxima exceeding 10^{-5} s^{-1} are identified and initialized into a set of tracks using a nearest neighbor search with a maximum displacement distance of 2° (geodesic, 222 km) in a time step. These are subsequently refined by minimizing a cost function for track smoothness. Only tracks that last longer than 1 day and travel more than 1,000 km are retained. Arctic cyclones are identified as those tracks with filtered $\xi_{850} > 8 \times 10^{-5}$ s^{-1} for at least 12 hr whilst located north of 70°N. For each track, only sections north of 55°N are retained (deemed relevant to the Arctic), from which time of maximum growth rate and maximum intensity are identified. There is no special treatment for merging/splitting tracks, as this introduces added subjectivity. Spatial track density of cyclones was computed with cosine-shaped kernels on a polar domain (500 km bandwidth) using the scikit-learn Python library (Pedregosa et al., 2011).

2.3. A Modified Cyclone Phase Space

A modified cyclone phase space for characterizing the structure of Arctic cyclones was proposed in Croad et al. (2023), adapted from Hart (2003). The modified phase space differs from the Hart (2003) version in that

the parameters have been non-dimensionalized by the natural scalings of quasi-geostrophic (QG) dynamics. The modified phase space has also been reduced from three to two dimensions for simplicity, considering the thermal asymmetry in the lower troposphere, and the thermal wind structure in the upper troposphere only, and not also in the lower troposphere as in Hart (2003). This is justified as we are primarily interested in the presence of low-level baroclinicity and TPVs in the upper levels. Furthermore, suitable pressure levels are used to define the layers in the modified phase space to account for the shallower troposphere in the Arctic. The modified phase space is also no longer dependent on the cyclone motion vector (as some Arctic cyclones are associated with slow movement such that the motion vector is not well defined), thereby producing smoother trajectories.

The thermal asymmetry is quantified as a non-dimensionalized depth-integrated baroclinic asymmetry, B, over the 925–700 hPa layer (assumed to be above the boundary layer but below the "steering" level), calculated by splitting the cyclone into two halves:

$$B = \frac{1}{f_0 L N} \frac{g}{\theta_0} \frac{1}{\Delta p} \int_{700hPa}^{925hPa} (\theta_R - \theta_L)\, dp \tag{1}$$

where f_0 = Coriolis parameter (s^{-1}), L = horizontal length scale (500 km), N = Brunt-Väisälä frequency (0.01 s^{-1}), g = gravitational acceleration (9.81 m s^{-2}), θ_0 = reference potential temperature (273 K), p = pressure (hPa), θ_R and θ_L = areal mean potential temperature over a semi-circle (radius 500 km) to the right and left side of the cyclone (K). At each time, (1) is calculated by splitting the cyclone at every 10° bearing, with the maximum value of B being used.

The thermal wind structure is quantified as a non-dimensionalized vertical gradient of relative vorticity (ξ; s^{-1}) in the 700–400 hPa layer (assumed to be above the "steering" level but below the tropopause):

$$Ro_T = -\frac{L}{N} \frac{\partial \xi}{\partial z} \tag{2}$$

where z = height (m) and Ro_T is a thermal Rossby number (the ratio of the vertical contrast in relative vorticity to planetary vorticity, noting that $\frac{L}{N} \sim \frac{H}{f_0}$ in QG scaling, where H = height scale). From thermal wind balance, a positive Ro_T indicates a warm-core structure, whilst a negative Ro_T corresponds to a cold-core structure.

In Croad et al. (2023), Equation 1 was calculated with data at 25 hPa intervals, and Equation 2 was estimated by a linear regression fit of ξ at 50 hPa intervals. However, here the parameters are calculated by finite difference using data at 925, 700 and 400 hPa only (reducing data storage requirements). Differences between the two methods were very small for the cyclone cases in Croad et al. (2023), justifying the decision to use fewer pressure levels.

The modified cyclone phase space is presented in Figure 1a, with four quadrants defined by the boundaries $Ro_T = 0$ and $B = 0.15$. The latter is equivalent to a ~2 K difference across a cyclone, above which a cyclone is considered to be asymmetric, and below which a cyclone is considered to be symmetric. This choice is justified a posteriori using the statistics at the time of maximum intensity shown in Figure 2b.

3. Results

3.1. Cyclone Structure and Evolution

During 1979–2021, 1,658 Arctic cyclones were identified in the extended summer (May–September) using the criteria in Section 2.2 (≈39 per year on average). All (6-hourly) tracked points of these cyclones are presented in the modified phase space in Figure 1a. The highest point density is in the lower-left quadrant (39.8%), indicative of cold-core cyclone structures with low asymmetry. There are also a considerable number of points in the top two quadrants, with 29.0% and 23.5% exhibiting warm-core and cold-core cyclone structures respectively with high asymmetry. The region of highest point density slants from the lower-left to the upper-right, indicating that cyclones with warm-core structures typically have greater low-level asymmetry than cold-core cyclones.

The sample is split into two subsets, depending on whether a cyclone is LLD (i.e., warm-core; $Ro_T > 0$) or ULD (i.e., cold-core; $Ro_T < 0$) at the time of maximum growth rate (Figures 1b and 1c). 65.5% (1,086) of the cyclones are LLD at maximum growth rate, whilst 34.5% (572) are ULD. Note that this partition is similar to that of cyclones that are unmatched and matched with TPVs in Gray et al. (2021). The LLD cyclones (Figure 1b) have a higher proportion of warm-core asymmetric structures than climatology (38.3% compared to 29.0%), and a lower fraction of cold-core structures. In contrast, the ULD subset (Figure 1c) has a considerably lower fraction of warm-core asymmetric structures than climatology (14.4% compared to 29.0%), with the region of highest point

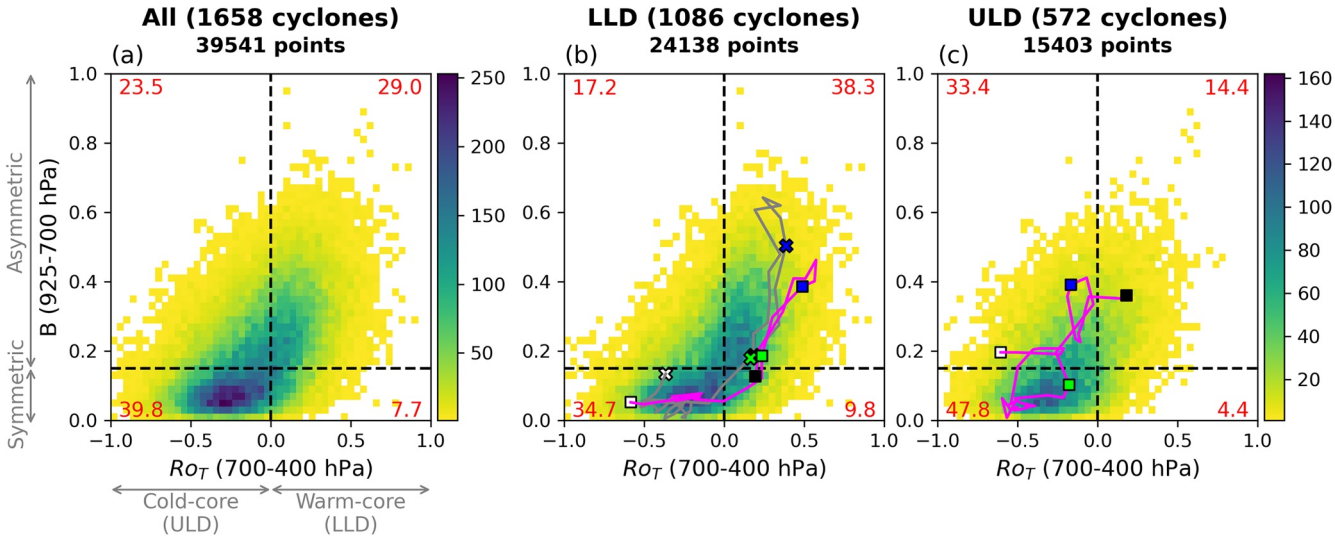

Figure 1. Point density in the modified cyclone phase space of all track points for (a) all, (b) LLD, and (c) ULD Arctic cyclones. Overlaid are the trajectories of three cyclone case studies; C12 and C20A are overlain on (b) in gray and magenta respectively, and C20B is overlain on (c) in magenta. The black, blue, green and white markers (crosses for C12, squares for C20A and C20B) refer to the start point, maximum growth rate, maximum intensity and final point respectively. The percentage of the total points in each quadrant is written in red.

density on the cold-core half of the phase space (and lower average asymmetry). The ULD subset has a higher proportion of cold-core asymmetric (33.4% compared to 23.5%) and cold-core symmetric (47.8% compared to 39.8%) structures than climatology.

The trajectories of the three aforementioned Arctic cyclone cases are overlaid in Figures 1b and 1c. C12 and C20A (Figure 1b; LLD development) have warm-core asymmetric structures at maximum growth rate (blue marker), with a reduction in asymmetry as they approach maximum intensity (green markers). After maximum intensity, the cyclone trajectories move into the lower-left quadrant, illustrating the transition to a cold-core axisymmetric structure, and remain there for several days. In contrast, C20B (Figure 1c; ULD development) has a cold-core structure at maximum growth rate, with high asymmetry (reduced compared to C12 but comparable to C20A). Although C20B has a contrasting development to C12 and C20A, it undergoes a transition around the time of maximum intensity to a cold-core symmetric structure that persists for several days, like C12 and C20A.

The evolution of structure throughout cyclone lifetime is highlighted in Figure 2. Considering the full cyclone sample, at maximum growth rate (Figure 2a), the highest point density is in the warm-core asymmetric (60.0%) and cold-core asymmetric (30.5%) quadrants. At maximum intensity (Figure 2b), the highest point density has moved to the left and downwards in the diagram, positioned on the central point between the quadrants, representing a reduction in asymmetry and a reduction in the fraction of warm-core structures as cyclones mature. At the final track point (Figure 2c), the highest point density is in the cold-core symmetric quadrant (62.0%). This represents the transition to a cold-core axisymmetric structure, like that seen in C12, C20A and C20B. The results indicate that a transition to a cold-core axisymmetric structure after maximum intensity occurs commonly in summer-time Arctic cyclones, consistent with Vessey et al. (2022).

Note that the highest point density at maximum growth rate (Figure 2a) is unimodal, even though in this study the cyclones are partitioned into two types depending on their structure at this time. This illustrates how in reality, cyclone structure is a continuum, rather than being constrained by distinct types (with many "unconventional" cyclones). However, it is still useful to apply broad classification schemes for the purpose of understanding characteristic cyclone structures and behaviors. The merit of this classification scheme is demonstrated in Figure 1, with the LLD and ULD subsets exhibiting different characteristic structures.

Figures 2d–2f and 2g–2i show the evolution of the LLD and ULD subsets respectively. At maximum growth rate, the LLD (Figure 2d) and ULD (Figure 2g) subsets have warm-core and cold-core structures respectively, by definition, with high asymmetry. At maximum intensity, the highest point density has moved downwards in the phase space in both subsets (Figures 2e and 2h), indicating reduced asymmetry as the cyclones mature. The LLD subset (Figure 2e) also moves to lower Ro_T values, although 67.7% of the cyclones still have warm-core structures

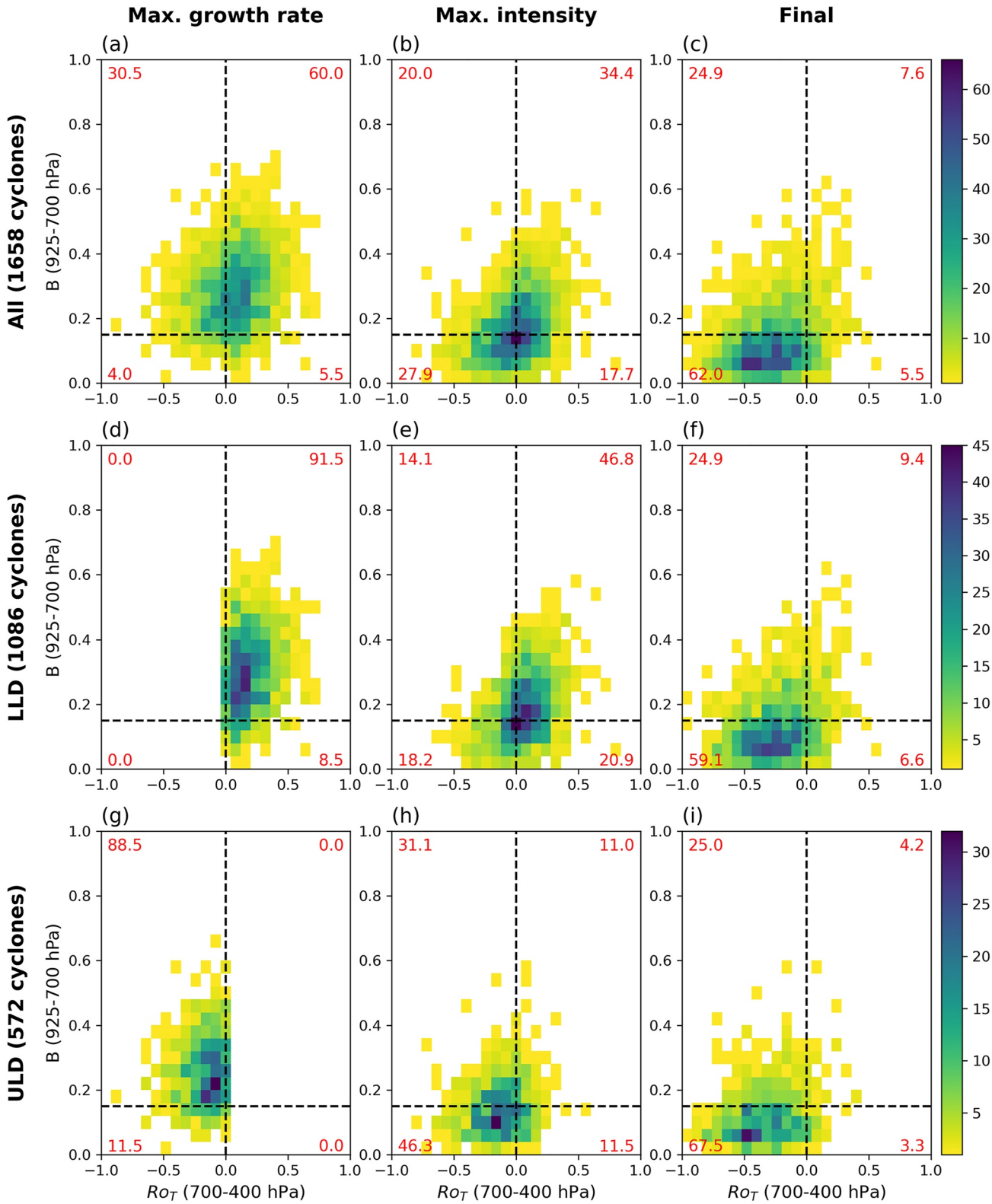

Figure 2. Point density in the modified cyclone phase space for (a–c) all identified Arctic cyclones at (a) maximum growth rate, (b) maximum intensity, and (c) the final point of each track. Panels (d–f) and (g–i) are the same as panels (a–c), but for LLD and ULD cyclones respectively. The percentage of the total points in each quadrant is written in red.

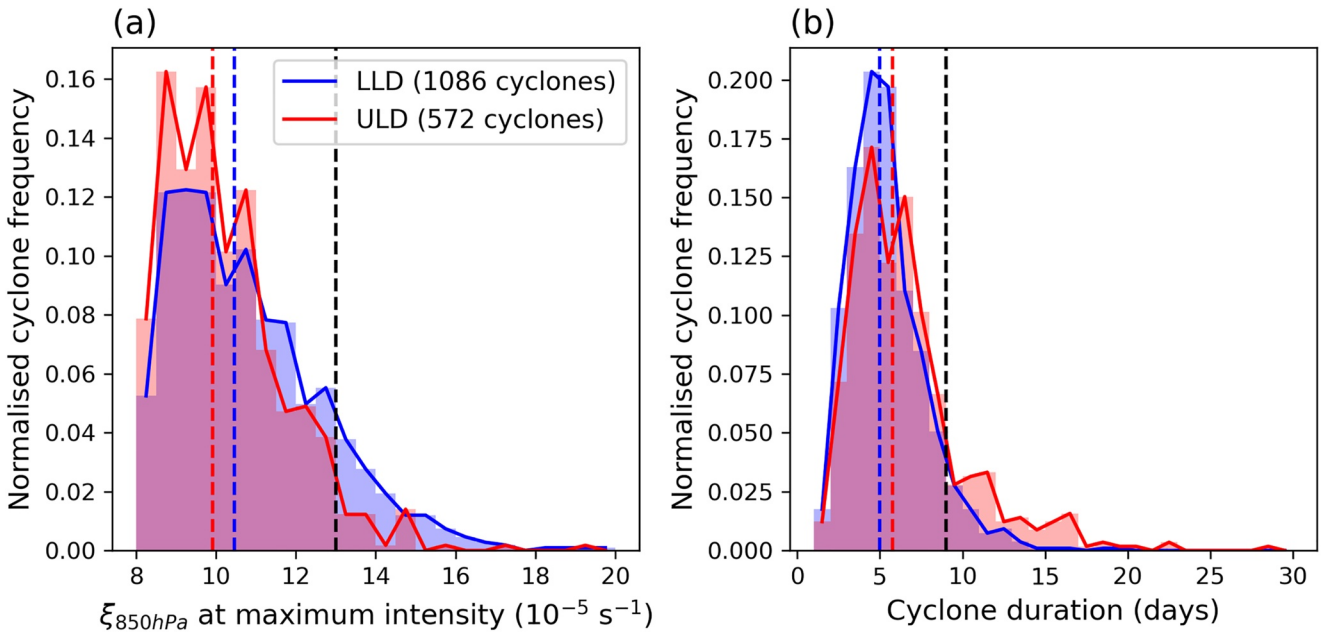

Figure 3. Histograms of Arctic cyclone (a) maximum strength according to ξ_{850} at maximum intensity and (b) duration, partitioned into the LLD (blue) and ULD (red) subsets. The histograms are normalized by the number of cyclones in each subset. The blue and red vertical dashed lines mark the median value for the LLD and ULD subsets respectively. The black vertical dashed line marks the 90th percentile value of all the cyclones.

at this time. This demonstrates that LLD cyclones tend to undergo their transition from warm-core to cold-core structures after maximum intensity, like C12 and C20A (Figure 1b). At the final track point, the LLD (Figure 2f) and ULD (Figure 2i) subsets have their highest point density in the cold-core symmetric quadrant, with 59.1% and 67.5% of the points respectively. This suggests that both LLD and ULD cyclones often undergo the transition to a cold-core axisymmetric structure, although a cyclone that had a ULD development is more likely to do so.

3.2. Cyclone Characteristics

Having illustrated the differences in structural evolution between LLD and ULD cyclones, we now consider how the cyclone subsets compare with regards to strength and duration (Figure 3).

The distributions of maximum strength for the LLD and ULD cyclones are presented in Figure 3a. The median value of ξ_{850} at maximum intensity (denoted by the dashed vertical lines) is higher for LLD cyclones (10.5×10^{-5} s^{-1}) than ULD cyclones (9.9×10^{-5} s^{-1}). Furthermore, the ULD histogram has a higher peak at low values of ξ_{850} compared to the LLD histogram, which is flatter in shape and has higher frequencies at larger ξ_{850} values. A two-sample Kolmogorov-Smirnov (KS) test confirms that the two distributions are robustly different (p-value $= 2.6 \times 10^{-7}$). This demonstrates that LLD cyclones are typically stronger than ULD cyclones, and that the strongest cyclones are more likely to have a LLD development.

An equivalent analysis is provided in Figure 3b for cyclone lifetime. The median duration is greater for ULD cyclones (6 days) than LLD cyclones (5 days). Moreover, the LLD histogram has a higher peak at short durations compared to the ULD histogram, which has a longer tail and higher frequencies at longer durations. A two-sample KS test confirms that the distributions are robustly different (p-value $= 3.8 \times 10^{-10}$). This demonstrates that ULD cyclones tend to be longer-lived than LLD cyclones, and, that the longest-lived cyclones are more likely to have an ULD development.

3.3. Extreme Cyclones

Here we focus on the cyclones that exceed the 90th percentile in strength and duration, which were found to be 13.0×10^{-5} s^{-1} and 9.0 days respectively (marked by the black vertical dashed lines in Figure 3).

The strongest cyclones subset is comprised predominantly of LLD cyclones (140; 12.9% of the LLD subset), with only 26 ULD cyclones (4.5% of the ULD subset). Accordingly, the distribution in the phase space (Figure 4a) resembles that of the LLD subset (Figure 1b). In contrast, the longest-lived cyclone subset is comprised of 67

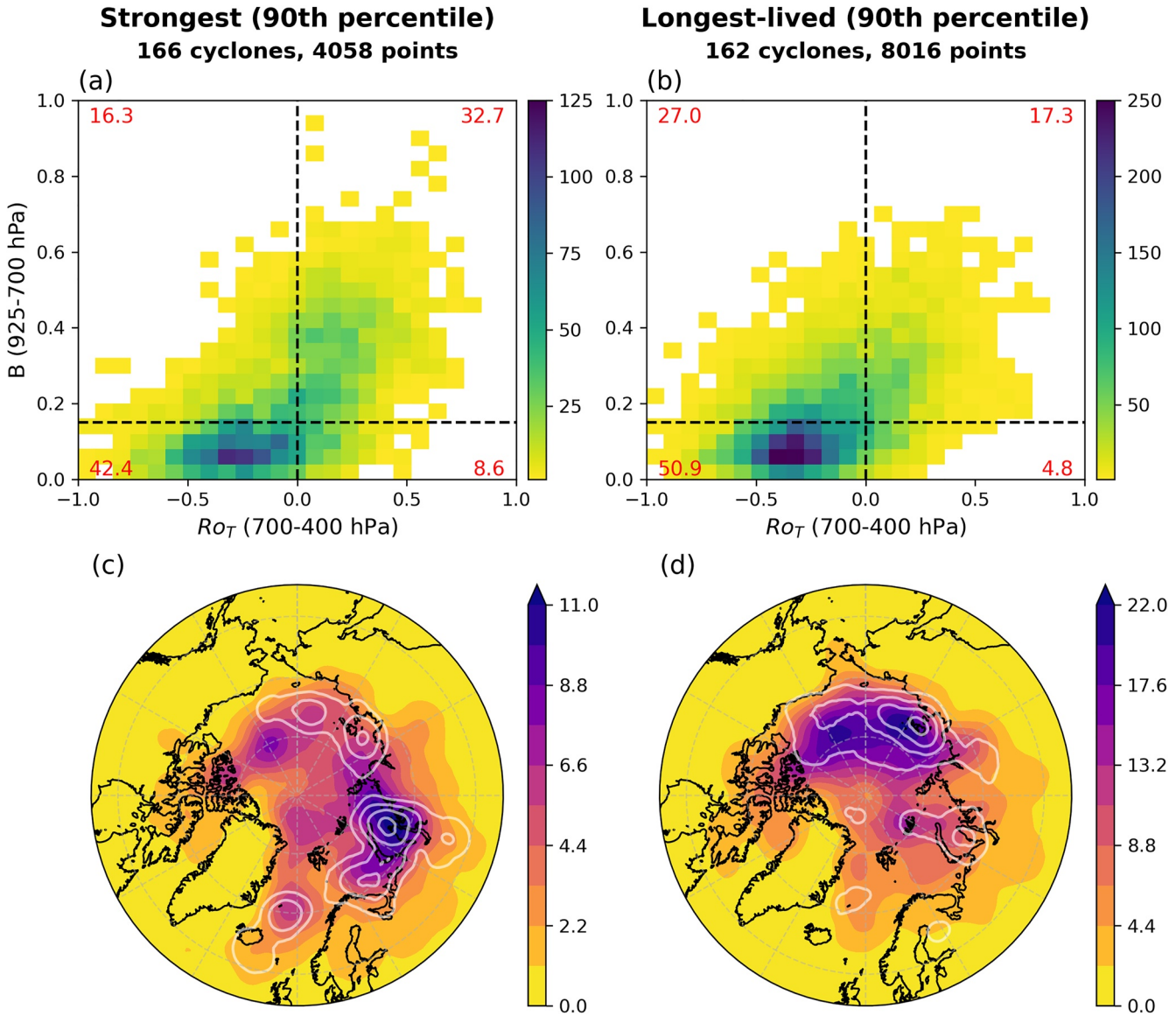

Figure 4. Arctic cyclones in the 90th percentile of strength (left) and duration (right). (Top) Density plots of the (a) strongest and (b) longest-lived cyclones in the modified cyclone phase space. (Bottom) Feature density maps (using spherical cosine kernels with 500 km bandwidth) of the (c) strongest and (d) longest-lived cyclone tracks for all track points (shading) and at the time of maximum growth rate (white contours at 0.2 intervals), with units of points per million km^2 per season.

LLD cyclones (6.2% of the LLD subset) and 95 ULD cyclones (16.6% of the ULD subset). The distribution in the phase space (Figure 4b) exhibits more cold-core structures than the strongest subset (Figure 4a), more closely resembling the ULD subset (Figure 1c). These results are consistent with LLD cyclones being stronger on average than ULD cyclones, and ULD cyclones being longer-lived. Both the strongest and longest-lived cyclone subsets have a greater fraction of cold-core axisymmetric structures than climatology (42.4% and 50.9% respectively compared to 39.8%). This is likely related to longer persistence after maximum intensity, either due to stronger cyclones taking longer to dissipate, or due to cyclones being maintained by upper-level forcing. Note that only 17 cyclones (~10% of the sample size) are in both the strongest and longest-lived subsets, suggesting that extremely strong cyclones do not tend to be extremely long-lived.

The strongest cyclones most frequently develop and track in the Barents and Kara Seas (Figure 4c), consistent with baroclinic development on the AFZ. Some of the strongest cyclones develop on the Laptev Sea coastline instead, highlighting a secondary baroclinic zone on the AFZ. In contrast, the longest-lived cyclones preferentially track in the Pacific sector of the Arctic Ocean, with a main development region in the Laptev and

East Siberian Seas that extends across the entire Pacific sector (Figure 4d). This suggests that the longest-lived cyclones tend to undergo baroclinic development on this eastern portion of the AFZ (i.e., distinct from the AFZ in the Barents/Kara Seas region). The Pacific sector is likely a hotspot for long-lived cyclones due to the proximity of this baroclinic zone with TPVs, which mostly commonly occur in this region (Cavallo & Hakim, 2010). The track densities of cyclones that are matched and unmatched with TPVs from Gray et al. (2021, Figures 7c and 7d respectively) are broadly similar to that of the longest-lived (Figure 4d) and strongest (Figure 4c) cyclone subsets here, further suggesting a link with TPVs.

Generally speaking, the strongest cyclones tend to have LLD development, whilst the longest-lived cyclones tend to have ULD development. However, this is not true in all cases. For example, C12 had a LLD development, and is in the strongest subset, but it was also very long-lived (and in the longest-lived subset) due to interaction with a TPV. This highlights that processes outside of a cyclone's main development can be important. This is especially relevant to extremely long-lived cyclones in the summer-time Arctic. Cyclones in the Pacific sector may be longer-lived (regardless of structure during growth) as they are more likely to encounter TPVs. Cyclones that interact with TPVs (forming a cold-core columnar vortex) have more opportunity for complex track evolutions exhibiting periods of re-intensification later in the life cycle.

4. Conclusions

In this study we have performed a climatological analysis of summer-time (May-September) Arctic cyclone structure using ERA5 reanalysis (1979–2021), and a modified version of the Hart (2003) cyclone phase space. Motivated by the contrasting life cycles of some notable Arctic cyclone case studies, the focus was how structure at maximum growth rate relates to the subsequent evolution. The findings are summarized below, with reference to the research questions defined in Section 1:

1. Cold-core axisymmetric structures are the most common cyclone structure in the summer-time Arctic, accounting for 39.8% of the track points. Asymmetric warm-core (29.0%) and cold-core (23.5%) structures are also common.
2. Low-level-dominant (LLD; 65.5%) and upper-level-dominant (ULD; 34.5%) cyclones follow distinct developmental trajectories in the phase space. During growth, LLD cyclones exhibit warm-core asymmetric structures, whereas ULD cyclones have cold-core asymmetric structures. LLD cyclones tend to have greater asymmetry during growth. However, Arctic cyclones typically exhibit a characteristic transition to a cold-core axisymmetric structure after maturity, regardless of structure at maximum growth rate.
3. LLD cyclones are on average stronger, whilst the ULD cyclones tend to be longer-lived. The strongest cyclones (which are predominantly LLD) preferentially track on the northern coast of Russia, consistent with high baroclinicity on the AFZ. The longest-lived cyclones (typically ULD) tend to track over the Pacific side of the Arctic Ocean basin, likely related to the climatological location of TPVs near North America.

LLD and ULD cyclones have different characteristics consistent with the dominant growth mechanisms for each type. LLD cyclones grow on greater low-level baroclinicity (with weaker tropopause disturbances) and so the near-surface cyclone is strong, but only for a limited time whilst the low-level baroclinic environment exists. ULD cyclones are dominated by some upper-level disturbance (e.g., a TPV), such that the low-level baroclinicity might be weaker, but the system can be maintained for longer if the upper-level feature remains (which can be a considerable length of time for TPVs in the summer-time Arctic), and by the lower tropospheric processes described in Croad et al. (2023).

This article has proposed a classification scheme for Arctic cyclones, working toward conceptual models which are key for our understanding of cyclone characteristics and hazards. However, some cyclones do not fit into the proposed classification, and these unconventional cyclones may be prevalent in the summer-time Arctic due to the lack of dynamical forcing (i.e., wind shear) for dissipation. Future work should focus on establishing the processes acting in LLD and ULD cyclones. For example, it has been shown that summer-time Arctic cyclones often attain persistent cold-core axisymmetric structures after maturity. Croad et al. (2023) demonstrated that friction and sensible heat fluxes over sea ice contributed to the maintenance of the cold-core structures of Arctic cyclones in their mature stages, but more work is needed to quantify how large these effects are on cyclone strength and longevity.

Data Availability Statement

ECMWF ERA5 reanalysis (Hersbach et al., 2020) data are publicly available and were downloaded from the Copernicus Climate Change Service Climate Data Store (Hersbach et al., 2017). The TRACK algorithm (Hodges, 1994, 1995) is available on the University of Reading's Git repository (GitLab) at https://gitlab.act.reading.ac.uk/track/track (Hodges, 2021).

Acknowledgments
HLC acknowledges PhD studentship funding from SCENARIO Natural Environment Research Council (NERC) Doctoral Training Partnership grant NE/S007261/1, with co-supervision by SPEK and super-computing support from ECMWF. JM, BH, and AV were funded by the Arctic Summer-time Cyclones: Dynamics and Sea-Ice Interaction NERC standard grant NE/T006773/1. BH was also supported by the National Centre for Atmospheric Science, which is funded by NERC under contract R8/H12/83. The authors also acknowledge the ECWMF for the production of the ERA5 reanalysis data set.

References

Aizawa, T., & Tanaka, H. (2016). Axisymmetric structure of the long lasting summer Arctic cyclones. *Polar Science*, *10*(3), 192–198. https://doi.org/10.1016/j.polar.2016.02.002

Asplin, M. G., Galley, R., Barber, D. G., & Prinsenberg, S. (2012). Fracture of summer perennial sea ice by ocean swell as a result of Arctic storms. *Journal of Geophysical Research*, *117*(C6). https://doi.org/10.1029/2011jc007221

Babin, J., Lasserre, F., & Pic, P. (2020). Arctic shipping and polar seaways. In *Encyclopedia of water: Sciences, technology and society*. https://doi.org/10.1002/9781119300762.wsts0098

Bjerknes, J. (1919). On the structure of moving cyclones. *Monthly Weather Review*, *47*(2), 95–99. https://doi.org/10.1175/1520-0493(1919)47<95:otsomc>2.0.co;2

Cavallo, S. M., & Hakim, G. J. (2009). Potential vorticity diagnosis of a tropopause polar cyclone. *Monthly Weather Review*, *137*(4), 1358–1371. https://doi.org/10.1175/2008mwr2670.1

Cavallo, S. M., & Hakim, G. J. (2010). Composite structure of tropopause polar cyclones. *Monthly Weather Review*, *138*(10), 3840–3857. https://doi.org/10.1175/2010mwr3371.1

Croad, H. L., Methven, J., Harvey, B., Keeley, S. P. E., & Volonté, A. (2023). The role of boundary layer processes in summer-time Arctic cyclones. *Weather and Climate Dynamics*, *4*(3), 617–638. https://doi.org/10.5194/wcd-4-617-2023

Day, J. J., & Hodges, K. I. (2018). Growing land-sea temperature contrast and the intensification of Arctic cyclones. *Geophysical Research Letters*, *45*(8), 3673–3681. https://doi.org/10.1029/2018gl077587

Gray, S. L., Hodges, K. I., Vautrey, J. L., & Methven, J. (2021). The role of tropopause polar vortices in the intensification of summer Arctic cyclones. *Weather and Climate Dynamics*, *2*(4), 1303–1324. https://doi.org/10.5194/wcd-2-1303-2021

Hart, R. E. (2003). A cyclone phase space derived from thermal wind and thermal asymmetry. *Monthly Weather Review*, *131*(4), 585–616. https://doi.org/10.1175/1520-0493(2003)131<0585:acpsdf>2.0.co;2

Hersbach, H., Bell, B., Berrisford, P., Hirahara, S., Horányi, A., Muñoz-Sabater, J., et al. (2020). The ERA5 global reanalysis. *Quarterly Journal of Royal Meteorological Society*, *146*(730), 1999–2049. https://doi.org/10.1002/qj.3803

Hersbach, H., Bell, B., Berrisford, P., Hirahara, S., Horányi, A., Muñoz-Sabater, J., et al. (2017). Complete ERA5 from 1940: Fifth generation of ECMWF atmospheric reanalyses of the global climate. [dataset]. Copernicus Climate Change Service (C3S) Data Store (CDS). https://doi.org/10.24381/cds.143582cf

Hodges, K. (1994). A general method for tracking analysis and its application to meteorological data. *Monthly Weather Review*, *122*(11), 2573–2586. https://doi.org/10.1175/1520-0493(1994)122<2573:agmfta>2.0.co;2

Hodges, K. (1995). Feature tracking on the unit sphere. *Monthly Weather Review*, *123*(12), 3458–3465. https://doi.org/10.1175/1520-0493(1995)123<3458:ftotus>2.0.co;2

Hodges, K. (2021). TRACK tracking and analysis system for weather, climate and ocean data [code]. Gitlab. Retrieved from https://gitlab.act.reading.ac.uk/track/track

Li, X., Otsuka, N., & Brigham, L. W. (2021). Spatial and temporal variations of recent shipping along the northern sea route. *Polar Science*, *27*, 100569. https://doi.org/10.1016/j.polar.2020.100569

Lukovich, J. V., Stroeve, J. C., Crawford, A., Hamilton, L., Tsamados, M., Heorton, H., & Massonnet, F. (2021). Summer extreme cyclone impacts on Arctic sea ice. *Journal of Climate*, *34*(12), 4817–4834. https://doi.org/10.1175/jcli-d-19-0925.1

Pedregosa, F., Varoquaux, G., Gramfort, A., Michel, V., Thirion, B., Grisel, O., et al. (2011). Scikit-learn: Machine learning in Python. *Journal of Machine Learning Research*, *12*, 2825–2830.

Peng, L., Zhang, X., Kim, J.-H., Cho, K.-H., Kim, B.-M., Wang, Z., & Tang, H. (2021). Role of intense Arctic storm in accelerating summer sea ice melt: An in situ observational study. *Geophysical Research Letters*, *48*(8), e2021GL092714. https://doi.org/10.1029/2021gl092714

Serreze, M. C., Lynch, A. H., & Clark, M. P. (2001). The Arctic frontal zone as seen in the NCEP–NCAR reanalysis. *Journal of Climate*, *14*(7), 1550–1567. https://doi.org/10.1175/1520-0442(2001)014<1550:tafzas>2.0.co;2

Shapiro, M. A., & Keyser, D. (1990). Fronts, jet streams and the tropopause. In C. W. Newton & E. O. Holopainen (Eds.), *Extratropical cyclones: The Erik Palmén memorial volume* (pp. 167–191). American Meteorological Society. https://doi.org/10.1007/978-1-944970-33-8_10

Simmonds, I., & Rudeva, I. (2012). The great Arctic cyclone of august 2012. *Geophysical Research Letters*, *39*(23). https://doi.org/10.1029/2012gl054259

Tanaka, H. L., Yamagami, A., & Takahashi, S. (2012). The structure and behavior of the Arctic cyclone in summer analyzed by the JRA-25/JCDAS data. *Polar Science*, *6*(1), 55–69. https://doi.org/10.1016/j.polar.2012.03.001

Tao, W., Zhang, J., & Zhang, X. (2017). The role of stratosphere vortex downward intrusion in a long-lasting late-summer Arctic storm. *Quarterly Journal of Royal Meteorological Society*, *143*(705), 1953–1966. https://doi.org/10.1002/qj.3055

Thomson, J., & Rogers, W. E. (2014). Swell and sea in the emerging Arctic ocean. *Geophysical Research Letters*, *41*(9), 3136–3140. https://doi.org/10.1002/2014gl059983

Vessey, A. F., Hodges, K. I., Shaffrey, L. C., & Day, J. J. (2020). An inter-comparison of Arctic synoptic scale storms between four global reanalysis datasets. *Climate Dynamics*, *54*(5), 2777–2795. https://doi.org/10.1007/s00382-020-05142-4

Vessey, A. F., Hodges, K. I., Shaffrey, L. C., & Day, J. J. (2022). The composite development and structure of intense synoptic-scale Arctic cyclones. *Weather and Climate Dynamics*, *3*(3), 1097–1112. https://doi.org/10.5194/wcd-3-1097-2022

Waseda, T., Nose, T., Kodaira, T., Sasmal, K., & Webb, A. (2021). Climatic trends of extreme wave events caused by Arctic cyclones in the western Arctic ocean. *Polar Science*, *27*, 100625. https://doi.org/10.1016/j.polar.2020.100625

Waseda, T., Webb, A., Sato, K., Inoue, J., Kohout, A., Penrose, B., & Penrose, S. (2018). Correlated increase of high ocean waves and winds in the ice-free waters of the Arctic ocean. *Scientific Reports*, *8*(1), 4489. https://doi.org/10.1038/s41598-018-22500-9

Yamagami, A., Matsueda, M., & Tanaka, H. L. (2017). Extreme Arctic cyclone in august 2016. *Atmospheric Science Letters*, *18*(7), 307–314. https://doi.org/10.1002/asl.757

Zhang, X., Walsh, J. E., Zhang, J., Bhatt, U. S., & Ikeda, M. (2004). Climatology and interannual variability of Arctic cyclone activity: 1948–2002. *Journal of Climate*, *17*(12), 2300–2317. https://doi.org/10.1175/1520-0442(2004)017<2300:caivoa>2.0.co;2